

NON-CENSORED RIB FRACTURE DATA FROM DYNAMIC BELT LOADING TESTS ON THE HUMAN CADAVER THORAX

Stefan Duma

Joel Stitzel

Andrew Kemper

Craig McNally

Eric Kennedy

Virginia Tech – Wake Forest, Center for Injury Biomechanics
United States

Fumio Matsuoka

Toyota Motor Corporation

Paper Number 05-0360

ABSTRACT

The purpose of this paper is to present data from dynamic belt loading tests on the thorax of human cadavers where the exact timing of all rib fractures is known. In order to generate non-censored rib fracture data, a total of 47 strain gages were placed throughout the thorax of two human cadavers (1 male, 1 female). In order to simulate thoracic loading from a severe car crash, a table-top belt loading device was developed that utilizes a servo-hydraulic test machine to apply a dynamic input. The belt load pulse was configured to result in 40% chest compression through a 150 ms load and unload cycle. Potentiometers and accelerometers measured the chest compression and acceleration at three locations, load cells in line with the belt provided belt loads, and load cells on the posterior side of the thorax measured the reaction loads. The time histories of each strain gage were analyzed to determine the time of fracture which could then be compared directly to the reaction loads and chest displacements at that exact time, thereby creating a non-censored data set. In both cadavers, all fractures (20 for female and 12 for male) occurred within the first 35% compression of the thorax. As a general trend, the first series of fractures were on the left side of the thorax where the belt passed over the abdomen. The peak strain at failure ranged from 1.1 % to 2.5 %. By utilizing this technique, the exact timing of an injury level can be characterized relative to the mechanical parameters. For example, using rib fractures as the parameter for AIS scores in the female test, it is shown that AIS 1 injury occurs at a chest compression of 21%, AIS 2 at 22%, AIS 3 at 24 %, and AIS 4 at 34%.

INTRODUCTION

The vast majority of thoracic impact research has focused on developing global criteria for predicting injury. These include force, acceleration, and

displacement based criteria, as well as combinations of the above [5, 13, & 15]. Recent work has focused on the prediction of injury due to different restraint systems. For example, the increase in thoracic injury severity with increased age for a given occupant size, restraint type, and crash type is well documented [1, 5, 6, 7, 16 & 20]. The most common injury that occurs during sled tests with belted cadavers is rib fracture [4, 8 & 20]. Also, it is known that rib fracture patterns vary by restraint type [8]. Kent *et al.* [10] evaluated the injury predictive value of hard tissue criteria by varying restraint condition and found compression is the best indicator of fracture risk. Moreover, the noted that there is a significant effect on the fracture patterns due to belt only, airbag only, and combined belt and airbag loading.

Kent [9] also notes one of the problems with global methods used to develop thoracic injury criteria is that the criteria correlate with injury without necessarily being functionally related to injury, in contrast to stress and strain. This is the critical limitation of previous studies designed to develop global thoracic injury criteria. In summary, all previous studies aimed at determining thoracic injury criteria generally rely on the same set of cadaver impact tests, which all provide censored injury data. In other words, it is not possible to determine the exact loads, accelerations, or displacements at the time of fracture. Rather, one only knows that an injury occurred as some point during the impact test. In order to reduce this limitation, this study presents a method to generate non-censored rib fracture data. Although previous studies have shown the ability to detect selected rib fractures, no method has been successful at mapping the exact fracture timing of the entire thorax during dynamic belt loading. Therefore, the purpose of this study is to develop a method for determining non-censored rib fracture data and to present results from

dynamic belt loading tests on the human cadaver thorax using this method.

METHODS

Dynamic belt tests were performed on two cadavers (one male, one female) instrumented with 47 single axis and rosette strain gages on the ribs, sternum, and clavicle. The primary components of the belt loading system were a tensile testing machine (MTS 810, 22 kN, Eden Prairie, MN) and rigid loading table (Figure 1). The thorax of each cadaver was placed over a rigid plate that distributed the applied load over four load cells to measure the reaction loads of the thorax which were used to compensate for inertial effects. The 5 cm wide nylon

loading belt was situated 40° from the sagittal plane of the body. The orientation of the belt simulated a passenger side seat belt, going over the right clavicle and left side of the abdomen. A series of wire cables and pulleys connected the hydraulic piston to a Material Testing System (MTS 810, 22 kN, Eden Prairie, MN) used to load the cable/belt system at the desired rate. The locations of the pulleys were adjustable to accommodate cadavers of various sizes as well as to alter the angle of the belt relative to the table top. A slack reducer, connecting the primary wire rope to two secondary wire ropes, served to displace the ends of the loading belt equally, as well as remove slack from the system.

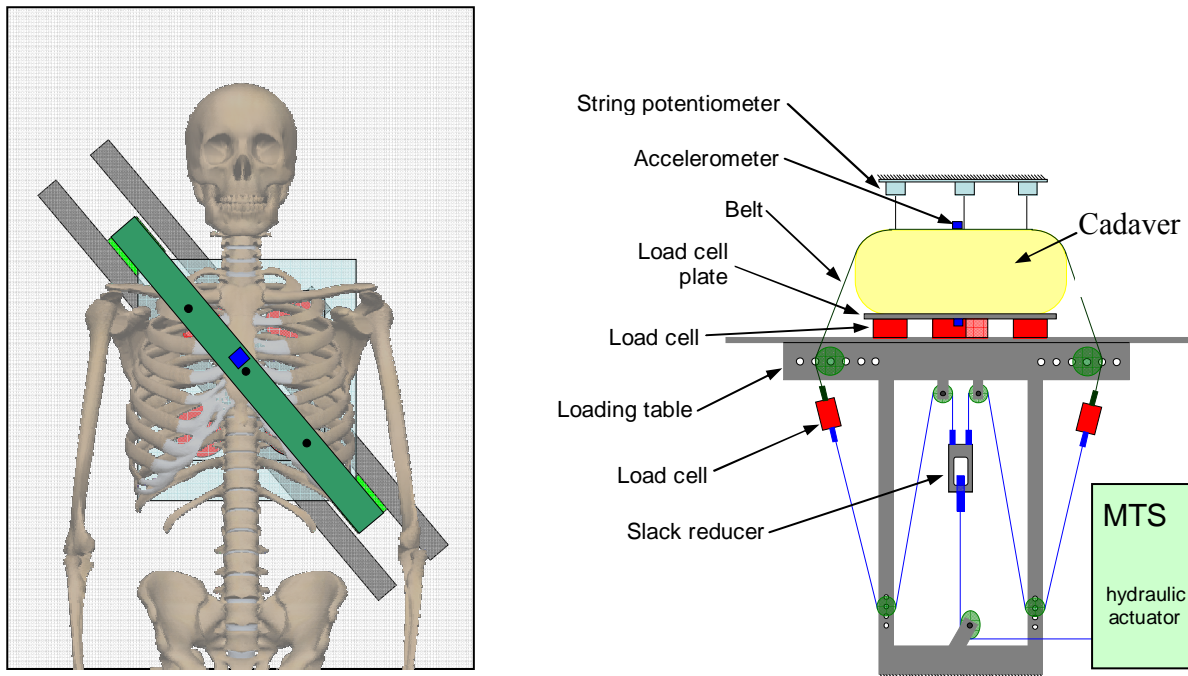


Figure 1. Top and Oblique View of Belt Loading System.

Once all the cables and instrumentation were connected, each cadaver was preconditioned prior to each test. This was done by placing a large flat 9.07 kg mass on the thorax five times for 10 seconds at one minute intervals. Before each test the MTS was used to pretension slightly the belt (75-80 N for the male, 58-75 N from the female). In order to model *in vivo* conditions, the test subjects' pulmonary systems were inflated to 14 kPa immediately prior to each test, which corresponded to the mean inspiration pressure, with a tracheostomy connected to pressure regulator. The depth of the inflated chest was then measured and recorded. Finally, the MTS machine

loaded the cable system at a rate of 1.5 m/s in order to simulate a severe car crash.

Instrumentation

Each cadaver was instrumented with a total of 47 strain gages; 26 single axial strain gages (Vishay Measurements Group, CEA-06-062UW-350, Malvern, PA) and 7 rectangular rosette strain gages (Vishay Measurements Group, CEA-06-062UR-350, Malvern, PA). The deflection of the thorax was measured using three string potentiometers (Space Age Control, 160, Palmdale, CA) that were attached

to the belt at the sternum and situated approximately 90 mm apart along the length of the belt (Figure 1). Additionally, an accelerometer (Endevco, 7264B, 2000 g, San Juan Capistrano, CA) was mounted on the belt at the sternum and load cell plate to acquire chest acceleration and table vibration. Belt tension was measured with two load cells (Interface, SSM-AJ, 13kN, Scottsdale, AZ). Four additional load cells (Denton, 5768, 11 kN, Rochester Hills, MI), (Denton, 1968, 22 kN, Rochester Hills, MI), (Denton, 1716A, 13 kN, Rochester Hills, MI) located between the cadaver and loading table, measured the force response of the body.

Test Subject Information

Two fresh frozen human cadavers were used in these tests (Table 1). It should be noted that chest depth measurements were taken from the middle of the sternum to the back of the thorax. Also, the percent compression was defined as the ratio of chest depth during the test to the chest depth measured prior to the test. For comparison with the standard population, Osteograms® were performed. The left hand of each cadaver was x-rayed and scanned by Compumed Incorporated (Los Angeles, CA). The BMD results are reported with respect to the normal population (Table 2). The t-score is used to compare the cadaver’s bone mineral density with that of the general population. The z-score is used to compare the bone mineral density of the female subjects with the average for their age. The t-score is expected to be low for these elderly cadavers with respect to the general population. A t-score of -1 corresponds to one standard deviation below the mean for the general population (30 year olds), meaning the individual is at or above the -63rd percentile for bone mineral density, or close to normal. T-scores of 2 and 3 correspond to 97th and 99th percentiles, respectively.

Table 2.
Subject Osteogram Results.

Cadaver Number	SM35	SF33
BMD Index	75.7	73.7
T-Score	-3.2	-3.4
Z-score	-1.4	-0.7

Table 1.
Subject Anthropometric Data.

Cadaver Number	SM35	SF33
Sex	Male	Female
Age	73	73
Weight	84.36 kg	45.35 kg
Height	154 cm	154 cm
Height (head to heal)	1730 mm	1540 mm
Sternum Length	210 mm	150 mm
Chest Circumference (Largest part)	1140 mm	700 mm
Chest Circumference (Center of Sternum)	1070 mm	740 mm
Linear Breadth (Center of Sternum)	370 mm	280 mm
Chest Depth (Center of Sternum)	230 mm	165 mm
Chest Circumference (Center of Thorax no Superficial Tissue)	840 mm	610 mm

Stain Gage Locations

The strain gages were located on the lateral sides of ribs 2-10 as well as the anterior side of ribs 3, 4, and 5 (Figures 2). The only difference between the two is the orientation of the rosettes on the left 7th and 9th ribs. The first “R” in the rib strain gage labels stands for “Rib”. Similarly, the first letters on the clavicle and sternum strain gage labels “CR”, “SU”, and “SL” stand for clavicle, upper sternum, and lower sternum respectively. The first number represents the number of the rib. The second letter “R” or “L” stands for the right side or left side of the thorax, respectively. The first letter after the dash, “S” or “R”, stands for single axis or rosette strain gage. The gages were numbered one to three bilaterally for ribs containing multiple gages. The number “1” gage corresponded to the gage closest to the sternum on each side, and the number “3” gage was the most distal gage from the sternum. The last letter “A”, “B”, or “C” only concerned the rosette strain gages and identifies the gage position within the rosette. For example, the strain gage label R3R-R3A stands for gage A of a rosette on the lateral right side of rib 3.

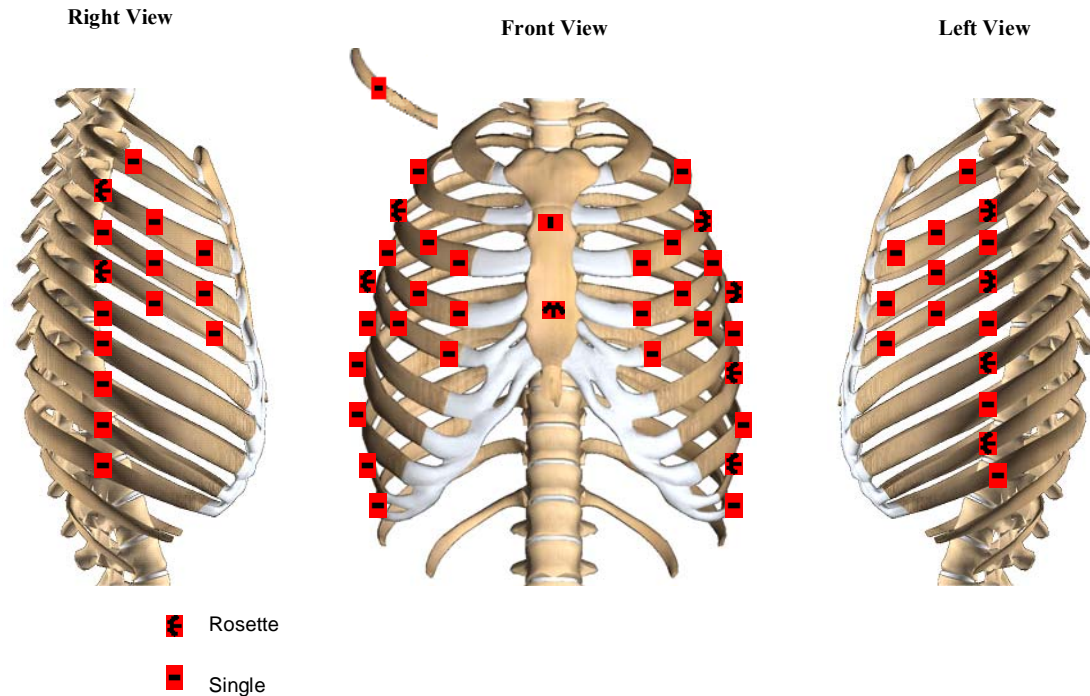


Figure 2. Strain Gage Positioning on the Thorax.

Strain Gage Attachment

Once the location of each strain gage was determined the surface of the bone was then swabbed with either and allowed to dry. Upon drying, Conditioner A an acidic solution, was applied to the surface with a clean piece of gauze in order to etch the surface of the bone. Then Neutralizer 5A a basic solution, was applied to the surface in order to neutralize the acidic solution. The gage was removed from its case and prepared by applying M-Bond Catalyst to the underside of the gage. Next, M-Bond 200 Adhesive was applied to the bone and the gage was quickly pushed over the adhesive in a rolling manner. The strain gage covered with a small piece of latex was held with firm pressure for 3 minutes (Figure 2.-7). Special care was taken to align each gage so that it was in line with the axis of the rib. The strain output from the three gages that composed each rosette was used to calculate the first and second principle strains and the angle Phi (Φ). Phi was defined as the angle from the gage reference axis (labeled X-Y) to the first principal axis.

RESULTS

In order to validate that these tests were representative of an actual sever crash, the data was

compared to data obtained from an actual sled test preformed (Figure 3). It can be seen that the compression rates produced from these tests closely match those seen in an actual sled test. The full travel of the MTS (15 cm) was used to fully compress the chest, causing 55% compression of the female thorax and 37% of the male thorax. This corresponded to 91.39 mm for the female and 100.36 mm for the male. The MTS was actuated at 150 cm/s, which compressed the thorax of the female at a rate of 94 cm/s and the male at 97 cm/s. The difference in the rate of the MTS and the rates seen by the cadavers was due to inertial effects and friction in the cable system.

The peak strains and strain rates vary from gage to gage for both the male and female cadavers (Table 3, Table 4). The highest absolute value for each gage was reported as the peak strain. The majority of the gages reported tensile loading. The strain rate was determined from the most linear portion of the initial strain loading. The majority of the gages reported tensile loading. The male cadaver had peak strain ranging from 1,533 to 39,812 (μ strain) in tension and from 1612 to 15,332 (μ strain) in compression. The female cadaver had peak strain ranging from 1,716 to 33,614 (μ strain) in tension and from 1,223 to 17,193 μ strain in compression. The rib strain rates seen by

the male cadaver ranged from -0.376 to 0.880 (strain/s), while strain rates seen by the female cadaver ranged from -0.468 to 0.547 (strain/s). The plots of strain vs. time for all the strain gages on both

the male and female are located in Appendixes A and B, respectively.

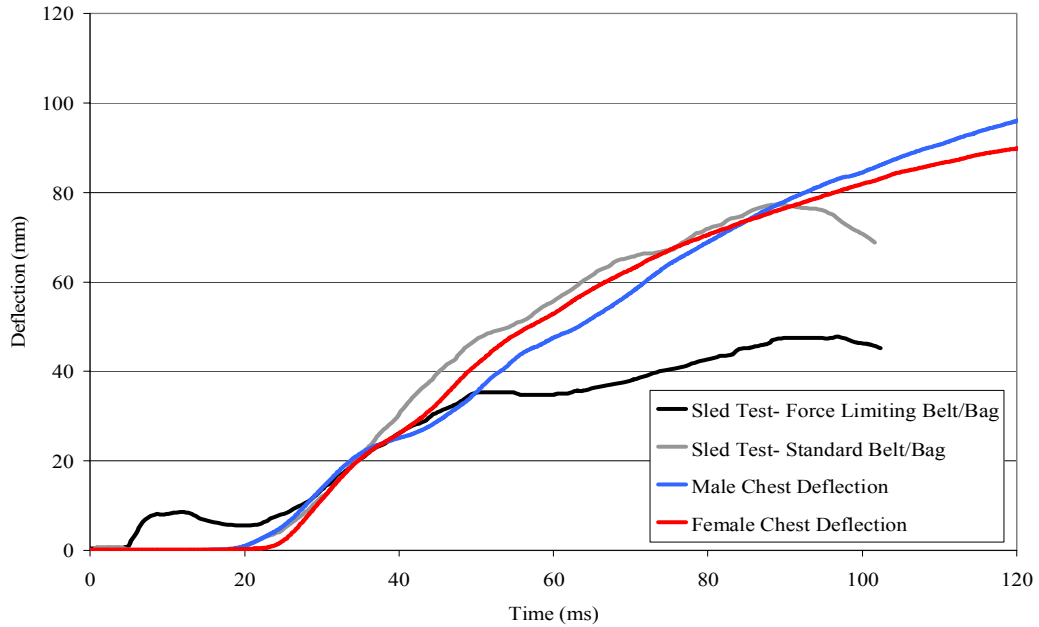


Figure 3. Chest Compression Rate of Cadavers in a 48 km/hr Sled Test (Kent, 2001) versus Presented Belt Loading Data.

Table 3.
Peak Strains and Strain Rates for all Strain Gages on Male Cadaver.

Strain Gage Number	Thorax Location	Rib Number	Gage Type	Rib Location	Peak Strain (μ strain)	Time (ms)	Strain Rate (strain/s)
R2R-S3	Right Side	2	Single	3	13680	79.3	0.243
R3R-S1	Right Side	3	Single	1	11353	89.5	0.134
R3R-S2	Right Side	3	Single	2	11595	89.2	0.209
R3R-R3A	Right Side	3	Rosette	3	1941	89.3	0.071
R3R-R3B	Right Side	3	Rosette	3	22111	88.9	0.459
R3R-R3C	Right Side	3	Rosette	3	12574	88.9	0.225
R4R-S1	Right Side	4	Single	1	5083	95.6	0.143
R4R-S2	Right Side	4	Single	2	13758	95.2	0.268
R4R-S3	Right Side	4	Single	3	12561	95.3	0.179
R5R-S1	Right Side	5	Single	1	4848	82.6	0.243
R5R-S2	Right Side	5	Single	2	7252	82.6	0.267
R5R-R3A	Right Side	5	Rosette	3	3335	82.9	0.054
R5R-R3B	Right Side	5	Rosette	3	8165	82.6	0.145
R5R-R3C	Right Side	5	Rosette	3	3577	82.6	0.055
R6R-S3	Right Side	6	Single	3	10480	136.2	0.095
R7R-S3	Right Side	7	Single	3	7014	132.3	0.080
R8R-S3	Right Side	8	Single	3	4557	132.7	0.062
R9R-S3	Right Side	9	Single	3	1286	118.2	0.015
R10R-S3	Right Side	10	Single	3	2810	121.5	0.079
CR-S3	Right Clavicle	N/A	Single	N/A	-6577	95.5	-0.122
SU-S	Upper Sternum	N/A	Single	N/A	-7711	69.1	-0.376
SL-RA	Lower Sternum	N/A	Rosette	N/A	13331	69.4	4.098
SL-RB	Lower Sternum	N/A	Rosette	N/A	39812	77.2	3.256
SL-RC	Lower Sternum	N/A	Rosette	N/A	7960	76.7	0.581
R2L-S3	Left Side	2	Single	3	11589	53.9	0.535
R3L-S1	Left Side	3	Single	2	10478	56.1	0.413
R3L-S2	Left Side	3	Single	3	13328	55.9	0.577
R3L-R3A	Left Side	3	Rosette	3	4624	55.9	0.172
R3L-R3B	Left Side	3	Rosette	3	5936	55.8	0.267
R3L-R3C	Left Side	3	Rosette	3	1839	56.1	0.144
R4L-S1	Left Side	4	Single	1	9290	51.4	0.449
R4L-S2	Left Side	4	Single	2	15576	51.4	0.880
R4L-S3	Left Side	4	Single	3	7948	51.5	0.410
R5L-S1	Left Side	5	Single	1	11741	47.3	0.603
R5L-S2	Left Side	5	Single	2	14128	47.3	0.706
R5L-R3A	Left Side	5	Rosette	3	3674	47.6	0.204
R5L-R3B	Left Side	5	Rosette	3	6499	47.6	0.342
R5L-R3C	Left Side	5	Rosette	3	1533	47.7	0.059
R6L-S3	Left Side	6	Single	3	6961	44.7	0.385
R7L-R3A	Left Side	7	Rosette	3	3772	42.6	0.215
R7L-R3B	Left Side	7	Rosette	3	6618	42.7	0.451
R7L-R3C	Left Side	7	Rosette	3	1822	117.1	0.117
R8L-S3	Left Side	8	Single	3	5080	136.0	0.318
R9L-R3A	Left Side	9	Rosette	3	2310	35.9	0.183
R9L-R3B	Left Side	9	Rosette	3	3026	35.8	0.251
R9L-R3C	Left Side	9	Rosette	3	-1673	52.7	-0.086
R10L-S3	Left Side	10	Single	3	-15332	126.1	-0.287

Table 4.
Peak Strains and Strain Rates for all Strain Gages on Female Cadaver.

Strain Gage Number	Thorax Location	Rib Number	Gage Type	Rib Location	Peak Strain (μ strain)	Time (ms)	Strain Rate (strain/s)
R2R-S3	Right Side	2	Single	3	-5504	111.2	0.138
R3R-S1	Right Side	3	Single	1	5508	85.8	0.300
R3R-S2	Right Side	3	Single	2	8000	111.1	0.191
R3R-R3A	Right Side	3	Rosette	3	2410	78.3	0.104
R3R-R3B	Right Side	3	Rosette	3	5246	57.2	0.225
R3R-R3C	Right Side	3	Rosette	3	4755	57.2	0.179
R4R-S1	Right Side	4	Single	1	3338	62.7	0.345
R4R-S2	Right Side	4	Single	2	7076	62.5	0.202
R4R-S3	Right Side	4	Single	3	5490	95.1	0.175
R5R-S1	Right Side	5	Single	1	2709	52.5	0.111
R5R-S2	Right Side	5	Single	2	4846	58.6	0.137
R5R-R3A	Right Side	5	Rosette	3	-1223	56.8	-0.044
R5R-R3B	Right Side	5	Rosette	3	7391	108.0	0.146
R5R-R3C	Right Side	5	Rosette	3	n/a	n/a	n/a
R6R-S3	Right Side	6	Single	3	10642	105.5	0.153
R7R-S3	Right Side	7	Single	3	7785	133.1	0.094
R8R-S3	Right Side	8	Single	3	4633	111.1	0.144
R9R-S3	Right Side	9	Single	3	2971	118.2	0.062
R10R-S3	Right Side	10	Single	3	1716	107.3	0.123
CR-S3	Right Clavicle	N/A	Single	N/A	-9020	74.4	-0.248
SU-S	Upper Sternum	N/A	Single	N/A	-2947	115.4	-0.195
SL-RA	Lower Sternum	N/A	Rosette	N/A	-2109	70.1	-0.058
SL-RB	Lower Sternum	N/A	Rosette	N/A	-7683	132.7	-0.316
SL-RC	Lower Sternum	N/A	Rosette	N/A	7729	84.2	0.300
R2L-S3	Left Side	2	Single	3	20681	72.8	0.531
R3L-S1	Left Side	3	Single	2	-8174	61.7	0.520
R3L-S2	Left Side	3	Single	3	33641	92.2	0.682
R3L-R3A	Left Side	3	Rosette	3	2593	119.7	0.034
R3L-R3B	Left Side	3	Rosette	3	3095	111.0	0.058
R3L-R3C	Left Side	3	Rosette	3	-3954	93.7	-0.069
R4L-S1	Left Side	4	Single	1	-7257	50.2	-0.301
R4L-S2	Left Side	4	Single	2	9028	49.1	0.385
R4L-S3	Left Side	4	Single	3	9139	49.2	0.350
R5L-S1	Left Side	5	Single	1	-17193	50.3	-0.468
R5L-S2	Left Side	5	Single	2	3008	45.5	0.129
R5L-R3A	Left Side	5	Rosette	3	6326	47.6	0.218
R5L-R3B	Left Side	5	Rosette	3	10109	47.5	0.460
R5L-R3C	Left Side	5	Rosette	3	7025	47.0	0.364
R6L-S3	Left Side	6	Single	3	12211	46.9	0.547
R7L-R3A	Left Side	7	Rosette	3	-3124	61.4	0.252
R7L-R3B	Left Side	7	Rosette	3	11357	46.1	0.491
R7L-R3C	Left Side	7	Rosette	3	8260	45.4	0.547
R8L-S3	Left Side	8	Single	3	-5254	51.7	0.275
R9L-R3A	Left Side	9	Rosette	3	n/a	n/a	n/a
R9L-R3B	Left Side	9	Rosette	3	-6217	621	0.320
R9L-R3C	Left Side	9	Rosette	3	3523	54.5	0.184
R10L-S3	Left Side	10	Single	3	9297	73.1	0.316

Rib Fracture Identification

The rib fractures locations were determined by performing a post-test injury analysis on each cadaver using a detailed necropsy of the thorax. The fracture locations were photographed and documented for each cadaver. The time of fracture was determined from the plots of strain gage output vs. time (Figure 4). The male cadaver sustained 12 fractures on 12 ribs [8 on the left, 4 on the right], as well as one fracture on the right clavicle (Figure 5). For the female cadaver, 20 rib fractures were detected on 12 ribs [14 on the left, 6 on the right] as well as one fracture to the sternum (Figure 6). The strain rates seen by the ribs of the male cadaver that fractured varied from 0.133 to 0.648 (strain/s), and from -0.581 to 0.559 (strain/s) for the female cadaver.

The male cadaver sustained two fractures directly under strain gages, and the female sustained 7. The fractures that occurred directly under gages are of particular interest because the peak strain at the time of fracture could be obtained from these gages.

In both cadavers, all rib fractures occurred within the first 35% compression of the thorax (Figure 7, Figure 8). As a general trend, the first series of fractures were on the left side of the thorax where the belt passed over the abdominal region. The ribs in the upper thoracic region on the right side fractured next.

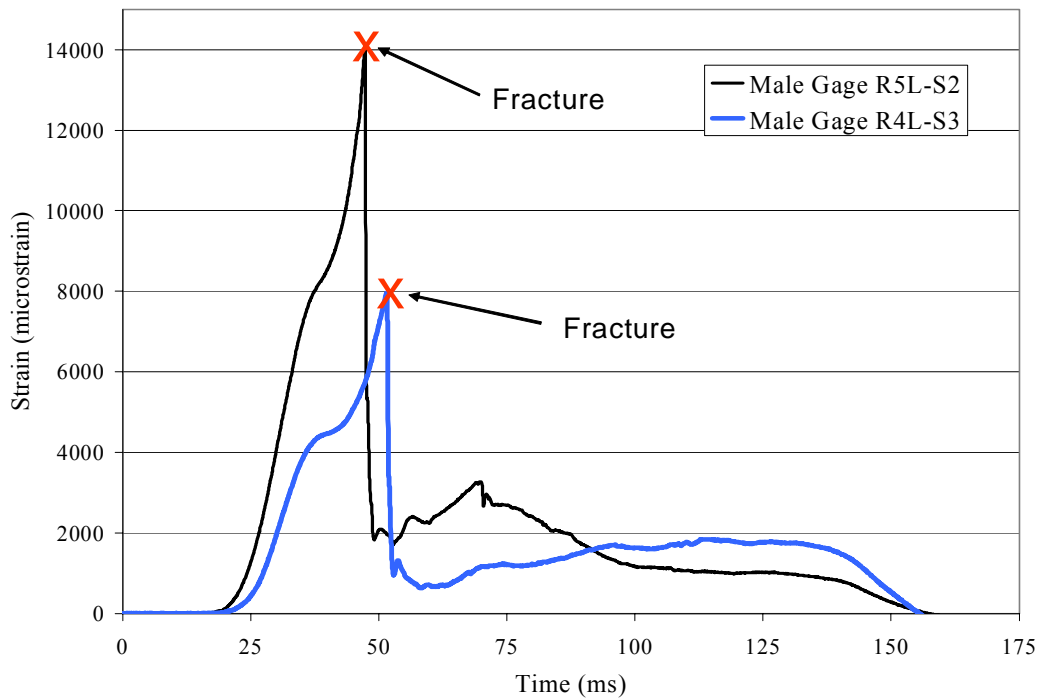


Figure 4. Determination of Rib Fracture Timing.

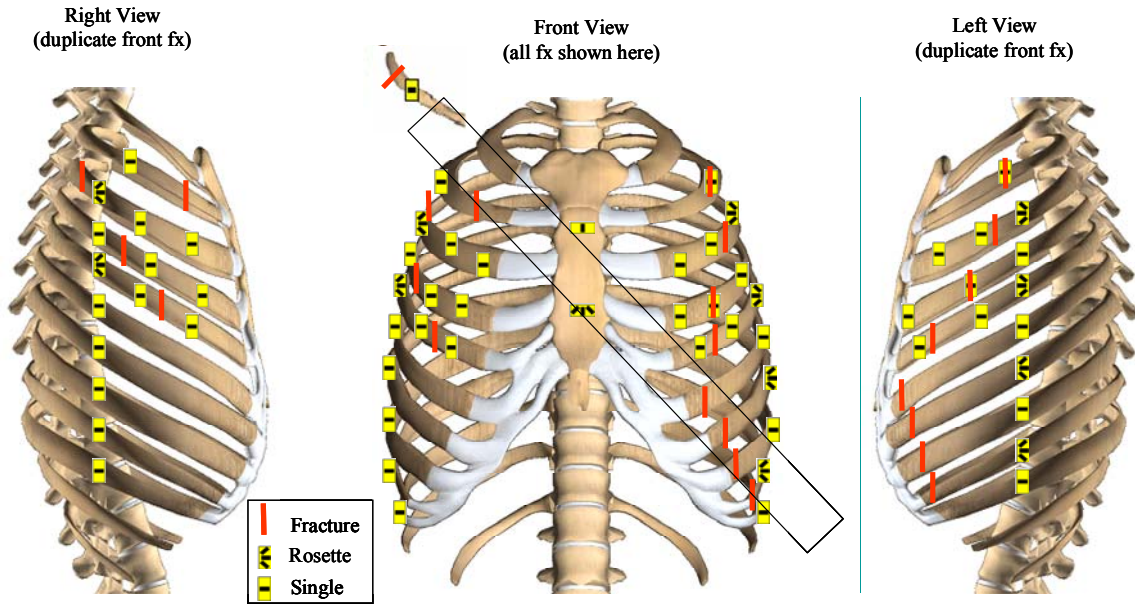


Figure 5. Location of Strain Gages and Fractures for Male Cadaver.

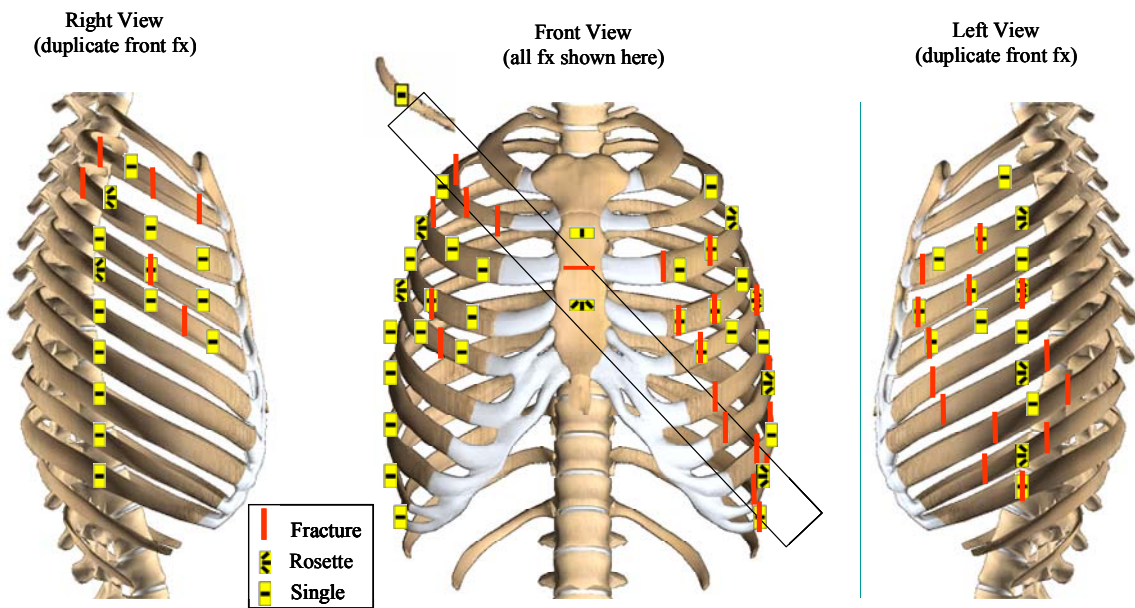


Figure 6. Location of Strain Gages and Fractures for Female Cadaver.

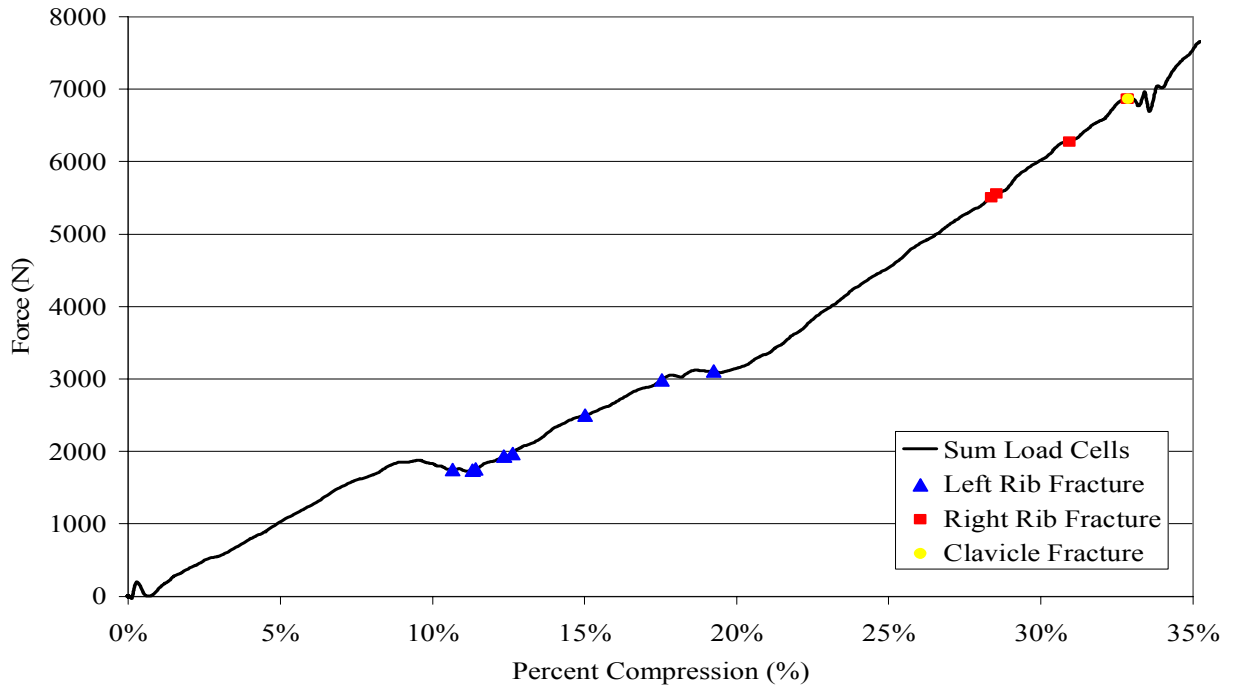


Figure 7. Rib Fracture Progression of Male Cadaver.

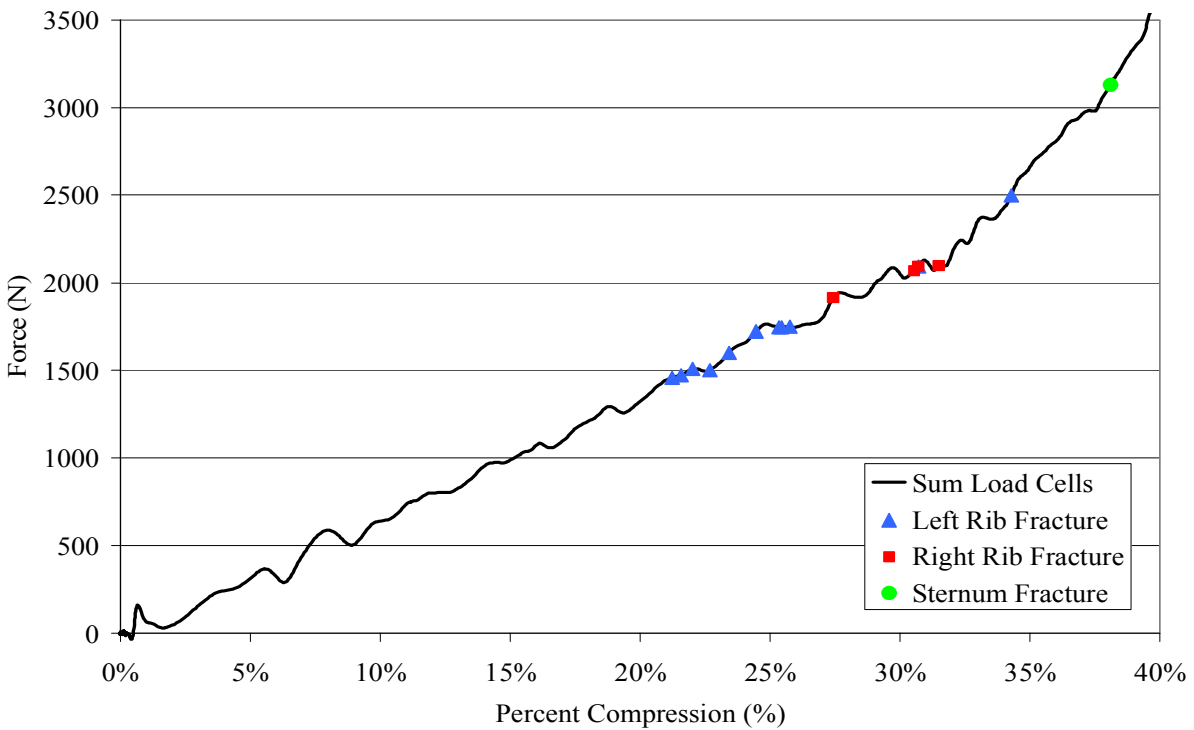


Figure 8. Rib Fracture Progression of Female Cadaver.

Principle Strain Results

The first principle strain, second principle strain, and the axial strain were plotted along with the angle from the axis of the rib to the first principal axis (Figure 9, Figure 10). In general, it was found that the first principle strain and the axial strain closely matched up to the time of the first fracture. In some cases the first principle strain and the axial strain continued to follow each other after the fracture and in other cases they did not. This could be due to either broken or damaged gages and or the complex loading seen after the fracture. The plots of first principle strain, second principle strain, axial strain, and theta for the other rosettes on the male and female cadavers are located in Appendixes A and B.

The maximum of the first and second principle strain before or at the first fracture were compared to the peak axial strain for each cadaver (Table 5, Table 6). The peak strains before or at the time of the first fracture were used because the strain could no longer be reported with confidence after the rib fractures due to the complexity of loading and possibility of damage to the gage. If no fracture occurred, then the strains reported were those that corresponded to the time at which the absolute maximum strain out of the three occurred. In some cases the rib was too small to adequately support all three gages of the rosette the data was suspect and thereby not reported in this section. Additionally, if one of more of the gages that composed each rosette broke during the test the data was omitted from this section.

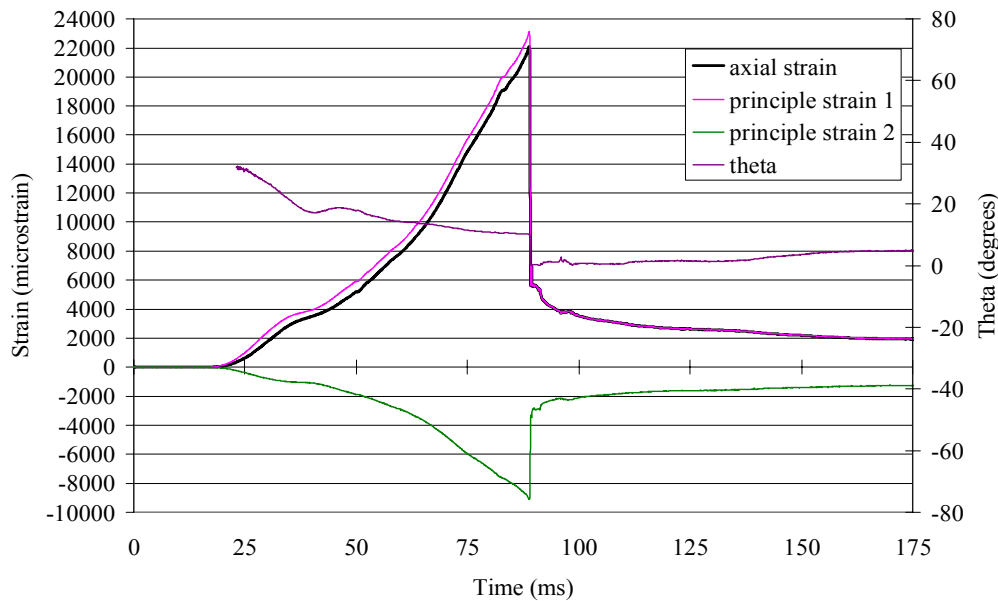


Figure 9.: Axial Strain, First and Second Principle Strain, and Theta vs. Time for Rosette R3R on the Male Cadaver.

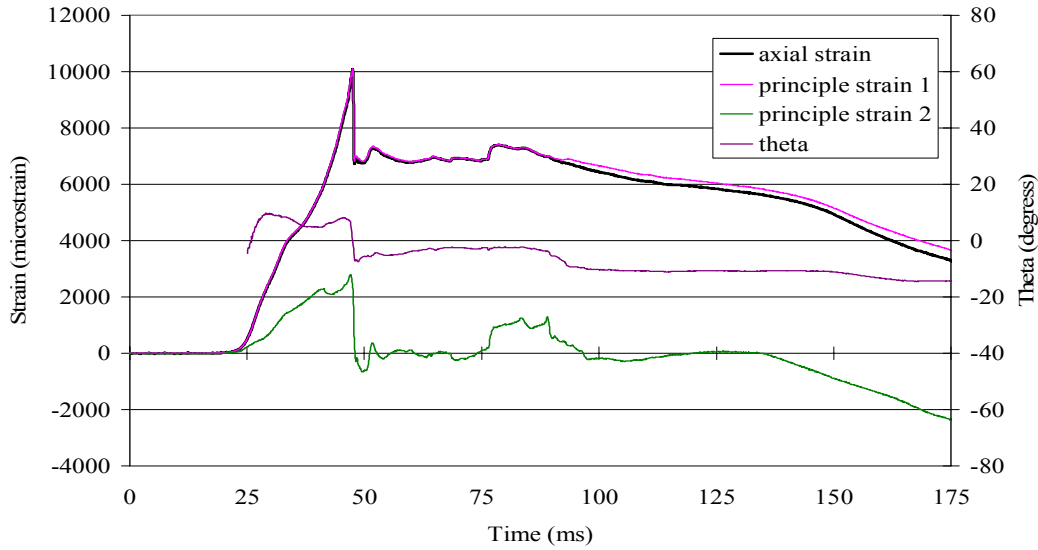


Figure 10. Axial Strain, First and Second Principle Strain, and Theta vs. Time for Rosette R5L on the Female Cadaver.

Table 5.

Comparison of Peak Axial Strain from Gage B of Rosette to Peak First Principle Strain for the Male Cadaver.

Rosette	Thorax Location		Peak Gage B Strain	Peak Principle Strain 1	Percent Difference	Peak Principle Strain 2	θ
R3R	Rib 3	Right Side	22111	23105	4.4	-8996	10.2
R5R	Rib 5	Right Side	8165	8223	0.7	-2465	3.8
R3L	Rib 3	Left Side	5890	6406	8.4	-636	-15.1
R5L	Rib 5	Left Side	6499	6661	2.5	-1605	-8.1
R7L	Rib 7	Left Side	6618	6773	2.3	-1792	-7.8
R9L	Rib 9	Left Side	3033*	3482*	13.8*	1844*	-17.0*

* = not measured at a time of fracture

Table 6.

Comparison of Peak Axial Strain from Gage B of Rosette to Peak First Principle Strain for the Female Cadaver.

Rosette	Thorax Location		Peak Gage B Strain	Peak Principle Strain 1	Percent Difference	Peak Principle Strain 2	θ
R3R	Rib 3	Right Side	5246	6142	15.7	-1581	19.9
R5R	Rib 5	Right Side	4641	4986	7.2	-3386	10.8
SL	Sternum	Lower	-4860*	12819*	444.3*	-5864*	76.6*
R3L	Rib 3	Left Side	2046	2325	12.8	-896	-18.1
R5L	Rib 5	Left Side	10109	10109	0.0	2735	0.1
R7L	Rib 7	Left Side	11357	11881	4.5	-674	12.6

* = not measured at a time of fracture

DISCUSSION

The reaction force data was plotted vs. percent chest deflection data for these tests with the fracture timing and corresponding Abbreviated Injury Scale (AIS) score (Figure 11, Figure 12). This was used to compare the definition of an AIS=3 for the human rib cage as defined by NHTSA to the injury criteria for an AIS=3 for the 50th percentile male and 5th percentile female hybrid III dummies. An AIS=3 for the rib cage was defined to be greater than 3 rib fractures on one side of the ribs and no more than 3 on the other side. NHTSA has defined the injury criteria of the 50th percentile male dummy as a chest

deflection of 63 mm, which corresponds to a 28%-30% percent chest deflection. The injury criteria for the 5th percentile female hybrid III dummy has been defined as a chest deflection of 52 mm which corresponds to a 22%-24% percent chest deflection. The range of percent chest deflections is due to the variations in dummy chest thickness as a result of tolerances set by the manufacturer, Denton ATD. As seen in Figures 4.2-1, and 4.2-2, an AIS= 3 occurred at 13% chest deflection for the male and 23% chest deflection for the female.

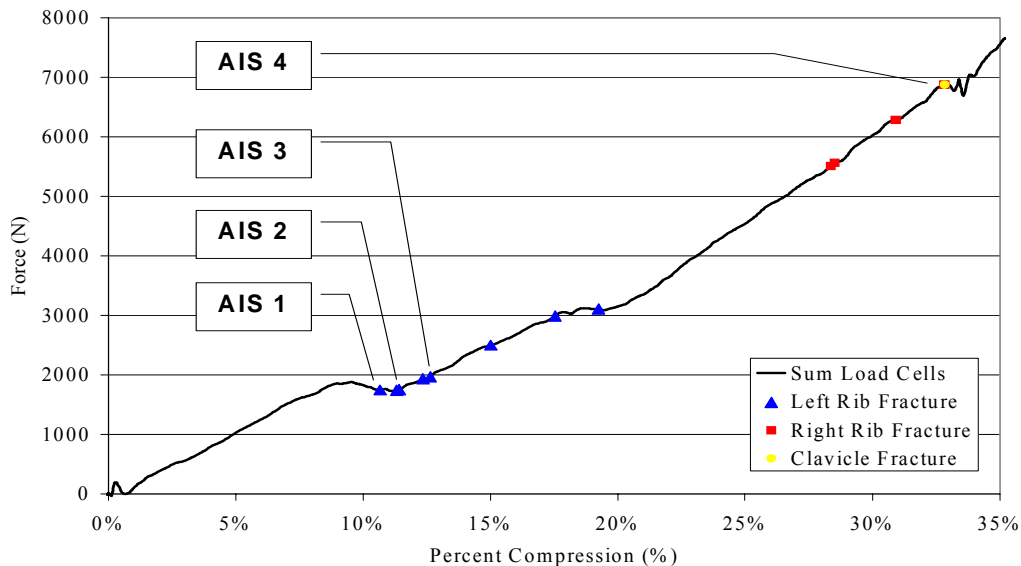


Figure 11. Rib Fracture Progression of Male Cadaver with AIS Levels.

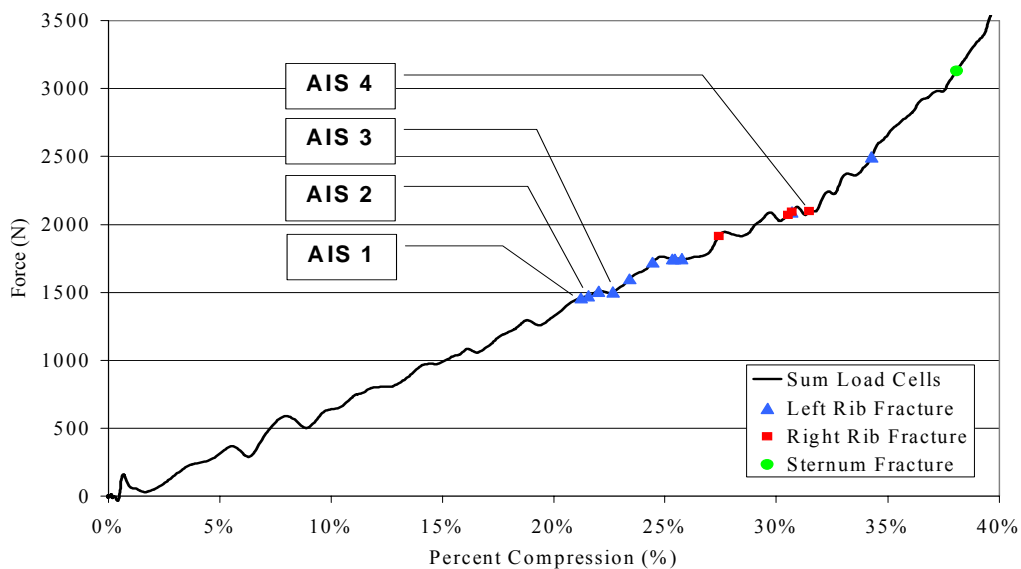


Figure 12. Rib Fracture Progression of Female Cadaver with AIS Levels.

Effective Stiffness

The thoracic testing conditions presented in this paper are similar to that presented by Kent [11] in that they present thoracic data due to diagonal belt loading at a rate that corresponds to the thoracic loading rate seen in a 48 km/h crash. Kent determined the effective stiffness of the thorax under these conditions by performing a linear regression of the force vs. percent deflection plots. These effective stiffness values for the male tests varied from 6,459-9,919 (N/ % deflection) and from 7,102-15,420 (N/ % deflection) for the female. The same method was performed on the force vs. percent compression data presented in his paper before the first fracture occurred. The effective stiffnesses for the male and female tests presented in the current study at Virginia Tech were 19,449 and 6,624 (N/ % deflection). However, there were large oscillations in the Kent data that were seen in the initial ramp up region of the force graphs such that the force fell below zero during these oscillations. This suggests a tension force while the thorax was being compressed. Therefore, the Kent data is likely lower than actual response during the initial loading phase.

CONCLUSIONS

The novel strain gaging technique presented in this report, in which the thorax was instrumented with the exception of a few gages, were usually the rosette element gages not aligned with the axis of the rib (i.e. gages A, and C), the clavicle gage, or the gages on the sternum.

The strain rates varied from gage to gage and from rib to rib for each cadaver. The strain rates sustained by the ribs ranged from -0.376 to 0.880 (strain/s) for the male cadaver and from -0.468 to 0.547 (strain/s) for the female cadaver.

The comparison of principle strain to axial strain resulted in four important findings. One, all the ribs with strain gage rosettes failed in tension. Second, the first principle strain was greater than or equal to the axis strain. However, the difference in values was small until the time of the fracture and therefore the value of theta (θ) was small. This meant that the direction of the first principle strain was not very far away from the axis of the rib. Third, the second principle strain was less than or equal to the axial strain, and in most cases was in negative (compression). Fourth, the confidence in the principle

with 47 single axis and rosette strain gages, has allowed for the precise determination of the time of fracture for each rib for the first time in the history of thoracic research. In addition, for the first time the exact point at which the different thoracic AIS scores occurred could be identified with the time of rib fracture data.

All rib fractures occurred within the first 35% compression of the thorax for both cadavers, and were side dependant for both cadavers. The first series of fractures were on the left side of the thorax where the belt passed over the abdominal region. The ribs on the upper right hand side of the thorax fractured second.

The effective thorax stiffnesses for the male and female cadavers presented in this paper were 19,449 and 6,624 (N/ % deflection) respectively, which were similar to values reported by Kent (2001). However, the data presented in this report is linear due to the robust design of the Virginia Tech belt tester, it does not have the problems of oscillations.

The strain gage data showed that majority of the ribs sustained tensile loading until the time of fracture. The male and female cadaver had peak tensile strains ranging from 1,533 to 39,812 (μ strain) and 1,716 to 33,614 (μ strain) respectively. The gages that showed predominately compressive loading, strain after fracture was low. This was due to the complex loading that occurred in the broken rib as well as the possibility of the damage that could have been sustained by the gage itself.

REFERENCES

- [1] Alem, N.M., Bowman, B.M., Melvin, J.W., and Benson, J.B. (1978) Whole-body human surrogate response to three-point harness restraint. *Stapp Car Crash Journal* 22: 361-399. SAE 780895.
- [2] Cesari, D. and Bouquet, R. (1990) Behavior of Human Surrogates under Belt Loading. *Proc. 34th Stapp Car Crash Conference*, pp. 73-82, Society of Automotive Engineers, Warrendale, PA.
- [3] Cesari, D. and Bouquet, R., (1994) Comparison of Hybrid III and Human Cadaver Thoracic Deformations." *Proceedings of the 38th Stapp Car Crash Conference*, Paper 942209, Society of Automotive Engineers, Warrendale, PA.

- [4] Crandall, J.R., Bass, C.R., Pilkey, W.D., Miller, H.J., Sikorski, J., and Wilkins, M. (1997) Thoracic response and injury with belt, driver side airbag and force limited belt restraint systems. *International Journal of Crashworthiness* 2(1): 119-132.
- [5] Eppinger, R.H. (1976) Prediction of thoracic injury using measurable experimental parameters. *Proc. 6th International Technical Conference on the Enhanced Safety of Vehicles: 770-779.*
- [6] Kallieris, D., and Mattern, R. (1979) Shoulder belt forces and thorax injuries. *Proc. 7th International Research Council on the Biomechanics of Impact: 171-183.*
- [7] . Kallieris, D., Schmidt, G., Barz, J., Mattern, R., and Schulz, F. (1974) Response and vulnerability of the human body at different impact velocities in simulated three-point belted cadaver tests. *Proc. 2nd International Research Council on the Biomechanics of Impact: 196-209*
- [8] Kallieris, D., Zerial, P.D., Rizzetti, A., and Mattern, R. (1998) Prediction of thoracic injuries in frontal collisions. *Proc. 18th International Technical Conference on the Enhanced Safety of Vehicles: 1550-1563.*
- [9] Kent, R.W. (2002) Dynamic response of the thorax: Restraint specific hard tissue injury. Ph.D. Dissertation, University of Virginia.
- [10] Kent, R.W., Crandall, J.R., Bolton, J., Prasad, P., Nusholtz, G.S., and Mertz, H.J. (2001) The influence of superficial soft tissues and restraint condition on thoracic skeletal injury prediction. *Stapp Car Crash Journal* 45: 183-204. SAE 2001-22-0008.
- [11] Kent R., Sherwood C., Lessley D., Overby B., (2003). Age-Related Changes in the Effective Stiffness of the Human Thorax Using Four Loading Conditions. *International Research Council on the Biomechanics of Impact, Lisbon Portugal.*
- [12] Kroell, C., Schneider, D., Nahum, A., (1974) Impact Tolerance and Response of the Human Thorax II. Paper number 741187, Society of Automotive Engineers, Warrendale, Pennsylvania.
- [13] Kuppa, S.M., and Eppinger, R.H. (1998) Development of an improved thoracic injury criterion. *Stapp Car Crash Journal* 42: 139-154. SAE 983153.
- [14] L'Abbe, R., Dainty, D., Newman, J., (1982) An Experimental Analysis of Thoracic Deflection Response to Belt Loading." *Proceedings of the 7th International Research Council on the Biomechanics of Impact Conference, Bron, France, pp. 184-194.*
- [15] Morgan, R.M., Eppinger, R.H., Haffner, M.P., Kallieris, D., Miltner, E., Mattern, R., Yoganandan, N., Pintar, F.A., Sances, A., Kuppa, S.M., Sharpless, C.L., Crandall, J.R., Pilkey, W.D., and Klopp, G.S. (1994) Thoracic trauma assessment formulations for restrained drivers in simulated frontal impacts. *Stapp Car Crash Journal* 38: 15-34. SAE 942206.
- [16] Patrick, L.M., Anderson, A., and Bohlin, N. (1974) Three-point harness accident and laboratory data comparison. *Stapp Car Crash Journal* 18: 201-282. SAE 741181.
- [17] Ramet, M., and Cesari, D. (1979) Behavior of restrained dummies and cadavers in frontal impacts. *Proc. 7th International Research Council on the Biomechanics of Impact: 210-219.*
- [18] Stitzel J.D., Cormier J. M., Barretta J.T., Kennedy E. A., (2003). Defining Regional Variation in the Material Properties of Human Rib Cortical Bone and its Effect on Fracture Prediction. *Stapp Car Journal, 47.*
- [19] Stitzel J.D., Cormier J. M., Barretta J.T., Kennedy E. A., (2003). Elderly Thorax Properties for Model Development. IBL Report Number 2003-020, Virginia Tech.
- [20] Viano, D.C. (1978) Thoracic injury potential. *Proc. 6th International Research Council on the Biomechanics of Impact: 142-156.*